Melt-spun Mg-Ni for Hydrogen Storage

By

Yuecheng Jin

School of Metallurgy and Materials

University of Birmingham

A thesis submitted to:

The University of Birmingham.

for the degree of:

MRes

School of Metallurgy & Materials

The University of Birmingham

September 2014

Abstract

Hydrogen energy has recently been considered as one of the most promising solutions to the emergence of sustainable and clean energy. However the storage of hydrogen still faces huge challenges. Therefore investigation of novel hydrogen storage materials has attracted a great deal of attention from both of the scientific and industrial communities.

It is believed that magnesium base alloys can be used for hydrogen storage because they can react with hydrogen to form magnesium hydrides, as well as their high hydrogen capacity, lightness, and low cost. Among several types of Mg base alloys, Mg-Ni alloys are of great interests due to its glass forming ability – amorphous structure, which can improve the hydrogen storage performance. In the present work, melt-spun technique has been used to synthesis Mg-Ni alloy with amorphous structure, and its hydrogen storage quality has also been analysed.

Mg-Ni alloy with nominal composition of Mg-10at.%Ni has been synthesised using melt-spun technique, and products with ribbon-shape have been obtained. The microstructure of the ingots has been characterised using scanning electron

microscope with energy dispersive spectrum. The crystal structure of the $Mg_{90}Ni_{10}$ sample has been determined using X-ray diffraction. Phase transformation during heating and cooling has been studied using differential scanning calorimetry in Ar and H_2 atmosphere. Hydrogen uptake capability has been investigated using intelligent gravimetric analyser. The effect of catalyst Nb_2O_5 has also been examined.

The present work has provided important information of using melt-spinning technique for synthesis of Mg-Ni alloy with amorphous structure. It also proves the potential of melt-spun Mg-Ni alloy as hydrogen storage material. Some future work is suggested on the basis of outputs in the present work, such as in-situ X-ray diffraction and hydrides formation/decomposition mechanism.

Acknowledgements

I want to express my gratitude to all the people who helped me through my project.

First of all, my supervisor Professor David Book helped me the most with my experiments and thesis, he was always willing to share his idea and provide his advice on many aspects. This work could not be done without his guide and expertise.

My special thanks go to my colleague and friend, Xiaodong, who provided valuable support to me in the lab, especially in the beginning of my experiments.

Also, many thanks go to all the colleagues from the Hydrogen Group, they patiently guided and supported me throughout these two years. It was very enjoyable working with them.

Finally and most importantly, I would like to thank all my lovely families during the course of my study.

Table of Contents

List of Figures

List of Tables

1. Introduction

The limited resource of fossil fuels and their damaging influence on the global environment has led to the rise in interest in the use of renewable energy. Among all the promising energy carriers, e.g. coal, natural gas, hydrogen and electrical batteries, hydrogen has a number of advantages, particularly for mobile applications. Due to the abundant resources, without the concern of running out of resources, it can be produced for sufficiently long period. In addition, the combustion of hydrogen and hydrogen fuel cells convert its chemical energy to electricity, heat and water, therefore the use of hydrogen is renewable, clean and non-toxic [1]. However, the presence of hydrogen as molecular gas is in a low-density state, which is a problem for the storage of hydrogen as a fuel. A possible solution for some hydrogen storage applications is based on hydride materials. Compared with molecular hydrogen either compressed to 100's of bar or cryogenically cooled to form liquid hydrogen, solid state hydrides (including metal/intermetallic hydrides and complex hydrides) give the highest volumetric hydrogen capacities without the problems of high pressures and thermal losses [2].

Mg and Mg-based alloys are particularly promising hydrides, as the theoretical hydrogen capacity of magnesium hydride (MgH_2) is 7.6 wt.% [3]. Moreover, its low density and reversibility are the key advantages as well as its abundance in

nature and low cost. However, both the hydrogen absorption and desorption rates need to be increased, and the release temperature reduced [4]. These two obstacles must be overcome in order to allow for it to be used in hydrogen stores. According to previous research, the hydriding properties of magnesium hydride can be improved by alloying with a number of transition metals, in particular Ni, and by introducing catalysts such as Nb_2O_5 [1]. Moreover, the development of nano-grained particles should result in accelerated sorption kinetics. There have been many attempts to try to produce the ideal nano-structured Mg-based alloy for use in hydrogen storage applications.

Various methods have been investigated to try to produce nano-structured materials for hydrogen storage, such as: ball milling, physical sputtering, and thermal evaporation [5]. This project will investigate melt-spinning, which is a rapid solidification process that can result in the production of amorphous and/or nano-crystalline alloys. The sample is loaded into a boron nitride or quartz crucible which has a nozzle at the bottom, from where the melted samples are ejected onto a spinning copper wheel with a surface velocity of up to 60 m/s. As the cooling rate ranges from 10^5 to 10^6 K/s, the formation and growth of grains is limited within such a short time period, while the nanocrystalline and amorphous phase(s) is formed as the ribbons are ejected. Typically, the thickness and width of the ribbons are 20-60 μm and 1-25 mm, respectively. The melting temperature,

vacuum level and surface velocity of the wheel can be controlled (Melt-spinner brochures).

This project will use a melt-spinning method to produce nano-structured Mg-Ni alloys. By optimising the nanostructures, examining the catalyst effect of Nb_2O_5 and surface modification, the major target is to improve the hydrogen storage properties of Mg-Ni alloys under acceptable temperature conditions.

2. Literature review

2.1 Sustainable hydrogen energy

In order to replace the fossil fuels and thus reduce the emission of green house gas emissions (such as CO_2), several sustainable energy strategies have been proposed since late 1990s. Many of these strategies have included the use of hydrogen energy technologies. The idea behind introducing hydrogen energy relates mainly to the challenges of pollution and energy security [6]. It has even been welcomed by some as the most possible solution to the problems of emergence of the new energy technology [7].

A common feature of the hydrogen and carbon cycles for energy use is that carbon or hydrogen does not play a major role in the underlying mechanisms of the cycle; rather, it is the compounds CO_2 and H_2O, respectively [8]. With a share of more than 80 % in total energy use in the transport sector, the automotive sector is the driving force for the introduction of hydrogen as fuel [9]. However, using hydrogen as a fuel brings technological problems, such as storage and distribution.

2.2 Hydrogen storage materials

2.2.1 Requirements for hydrogen storage

Although hydrogen may be an important energy vector in the future, to use hydrogen both in industry and daily life faces the technical challenge of storage.

Hydrogen is a molecular gas under standard conditions, and both its density and volumetric energy density are poor – 0.0909 kg/m^3 and 12.5 MJ/m^3, respectively. Storage and transportation of hydrogen in a pressurized gaseous state is possible using cylinders which have a: high tensile strength, low density, and good resistance to react with hydrogen. Normally the cylinders are under a pressure of roughly 200 – 300 bar [10]. The pressure can be increased to 350 – 700 bar using carbon fibre-reinforced cylinders [11, 12].

Alternatively, hydrogen gas can be transformed into a liquid for storage. The volumetric density and energy density can be greatly increased, while the process of liquefaction itself requires much higher energy. In addition, even in the best insulated dewar, the liquid hydrogen will eventually convert to a high-pressure gas ("boil-off"). Therefore the cost of liquid hydrogen storage is too high for most practical applications, with a few exceptions such as for the aerospace industry.

Solid-state hydrogen storage refers to the absorption of hydrogen into a material, which can then be released during service by changing the temperature or

pressure. One of the advantages is that distance between hydrogen atoms in side a hydride material, is much smaller than in molecular hydrogen. However, the gravimetric density is decreased due to the mass of the metals in the hydride.

For hydrogen fuel cell vehicles, hydrogen storage should enable a driving of about 300 miles, with short charge/recharge time at relatively low temperatures. The US Department of Energy (DOE) has announced new performance targets for hydrogen vehicles in 2009 [13], which is: 5.5 wt.% and 40 kg/m^3 H_2 by 2017; and 7.5 wt.% and 70 kg/m^3 H_2 as the ultimate targets. This indicates that materials for hydrogen storage must have:

(i) High storage capacity and gravimetric / volumetric densities;

(ii) Low reaction temperatures;

(iii) Fast sorption / desorption kinetics;

(iv) Long cycle life;

(v) Safe.

To date, no material has been found which fulfils all of the above requirements, and thus further research work is needed to investigate novel materials and synthesis / processing conditions.

2.2.2 Metal hydrides

Various types of metal hydrides have been investigated for hydrogen storage, including different elements and alloys such as: Pd [14], Ca, Mg [15], La-Ni [16], and Mg-Ni [17]. Transition metals or rare earth elements are usually added to form complex alloys.

2.2.3 Magnesium hydrides

Magnesium hydride has a relatively higher volumetric hydrogen storage density due to the light atomic weight of Mg. In addition, Mg can react with hydrogen reversibly and form the ionic compound MgH_2 ($Mg + H_2 \Leftrightarrow MgH_2$). Under standard conditions of temperature and pressure, the MgH_2 phase has a tetragonal crystal structure: α-MgH_2. This phase also has two other allotropes at high temperatures and pressures. One is β-MgH_2 with a hexagonal structure at 650 °C under 80 kbar [18]; and the other is γ-MgH_2 with an orthorhombic structure at 800 °C under 20 kbar [19].

The maximum gravimetric capacity of MgH_2 phase for hydrogen storage is 7.6 wt.% [20] and the energy density is 9 MJ/kg [21]. Such relatively high values for both the gravimetric capacity and energy density, may give opportunities for the application of magnesium hydrides for mobile hydrogen storage applications.

Hydrogen absorption into Mg is an exdothermic reaction: for $Mg + H_2 \rightarrow MgH_2$; ΔH = -74.5 kJ/mol [22]. Whereas, dehydrogenation of MgH_2 is an endothermic reaction.

However, despite the advantages described above, there are a number of problems that need to be solved: (i) reaction kinetics are slow in terms of the formation and decomposition of MgH_2 phase; and (ii) temperature required for hydrogen sorption is relatively high (~300 °C), in thermodynamic equilibrium under 1 bar pressure.

Since the diffusivity of hydrogen is slow within the MgH_2 phase, the formation and further growth of a MgH_2 layer at the Mg/H interface will decelerate the reaction between Mg and H_2, and thus decrease the sorption kinetics. Impurities and defects on the metal surface can accelerate hydrogen sorption; however pure magnesium with clean surface would need high energy in order to allow hydrogen absorption on the surface.

One possible solution is to replace pure magnesium with magnesium alloys / intermetallic compounds, e.g. Mg-Cu, Mg-Al, and Mg-Ni systems. The addition of alloy elements can not only decrease the enthalpy formation of corresponding

hydrides, but also introduce defects onto the particle surface, which consequently increase the reaction rates for hydrogen sorption and desorption.

2.2.4 Mg-Ni based hydrides

The potential use of Mg-Ni-based hydrides for hydrogen storage was first investigated by Reilly and Wiswall [17]. In their study, the intermetallic compound Mg_2NiH_4 was determined to have a tetragonal structure. Under 1 bar pressure, Mg_2Ni phase will react with hydrogen at about 250 – 280 °C to form the intermetallic compound Mg_2NiH_4:

$$1/2\ Mg_2Ni + H_2 \Leftrightarrow 1/2\ Mg_2NiH_4$$

the enthalpy of formation is -64.5 kJ/mol [17], significantly less than the -74.5 kJ/mol for pure magnesium. In their study it was also found that the ratio of H/(Mg+Ni) was about 0.1, and a short cycling activation process at room temperature was needed for a polycrystalline Mg_2Ni ingot. This study showed that Mg-Ni based hydrides can have lower hydrogen reaction temperatures and reasonable hydrogen storage capacity.

A comprehensive study on the relationship between nano-scale structures of Mg-Ni phases within the binary system and their hydriding properties, was carried out by Orimo and Fuji [3]. They studied nanostructured (also

nano-crystalline) Mg_2Ni, pure amorphous MgNi and a mixture of both, respectively.

(i) Grain boundary region was the key to the relationship between the nano-structure and the hydriding properties, which absorbed nearly 85 % of the total amount of hydrogen (1.6 wt.%). The dehydriding temperature under argon also dropped from 247-297 °C to 167 °C.

(ii) For the mixture of nanostructured Mg_2Ni and amorphous $Mg_{1-x}Ni_x$ (x=33, 38, 43, and 50 at.%), with increasing Ni concentration, the hydrogen capacity increased from 1.7 to 2.2 wt.% while the dehydriding temperature (under argon), decreased from 167 to 100 °C. Pure amorphous MgNi was found when the composition of Mg and Ni was equal (x=50 at.%) with the best hydrogen capacity (2.2 wt.%) and lowest dehydriding temperature (100 °C) under argon.

(iii) Although it was thought that $MgNi_2$ did not react with hydrogen, after mechanical milling to produce nano-scale grains, it was found to absorb 0.5 wt.% hydrogen at room temperature [3].

2.3 Techniques to improve hydrogen storage

2.3.1 Ball milling

To get amorphous and / or nanocrystalline Mg-based alloys with improved hydrogen storage performance, ball-milling is used widely and is a convenient

route for adding additives / catalyst according to Zaluska et. al. [23]. determined the properties of nanocrystalline magnesium produced by ball-milling. The hydrogen sorption kinetics of the ball-milled samples can undergo a remarkable improvement. Without any previous heat treatment or activation, over 6 wt.% hydrogen was absorbed by a 30 nm grained sample within 120 min, which is five times that for regular Mg powders. The temperature under which hydrogen absorption started also reduced from 400 to 300 °C. They also explained the role of the grain size on hydrogenation. In short, with decreasing grain size, more defects and grain boundaries were formed. Therefore, the nucleation of the hydride was accelerated as well as the penetration of hydrogen atoms through particles, and the formation of multi-crystal structure enabled hydrogen to diffuse through the imperfect hydride faster [24]. Yao et. al. determined the effect of grain size with the temperature-dependent coefficients, which was calculated by a theoretical model incorporating experiment data [25].

2.3.2 Melt-spinning

Unfortunately, after cycles of hydrogen absorption / desorption, the ball milled Mg-Ni hydride is not stable as the kinetics decrease significantly. It also takes a long time (over 2 hours of ball milling) to produce nanostructured materials. As demonstrated in many previous research, melt-spinning technology can solve the drawbacks mentioned above while provides better hydriding properties at

lower temperature, which makes it promising for mass-production of high purity amorphous and nanocrystalline Mg-base alloys [26]. Yim et. al. compared the hydriding properties of Mg-xNi (x=13.5, 23.5, 33.5 wt.%) produced by gravity cast, melt spinning with heat treatment afterwards. Results showed that the highest hydrogen capacity and best sorption kinetics were achieved by Mg-23.5%Ni that was heat-treated after melt spinning [27]. Spassov et. al. made different amorphous and nanocrystalline Mg-Ni alloys with small amounts of RE additives by melt spinning. Among all the samples, the nano-amorphous Mg75-Ni20-Mm5 absorbed about 3 wt.% in 10 minutes and then nearly 4 wt.% hydrogen within one hour [28]. The Mg-Ni and Mg-Ni-Y alloys, produced by Pohlmann et. al. using melt spinning, achieved up to 5.5 wt.% hydrogen capacity and 1.3 wt.% per minute hydrogen uptake velocity [29].

2.3.3 Activation

Thermal sorption cycling(s), adopted as an activation treatment, is often carried out at 300 °C in 10 ~ 20 bar hydrogen. This procedure has been found to improve the capability of hydrogen storage for melt-spun Mg-Ni base alloys. Tanaka et. al. [30] studied the melt-spun Mg-Ni-RE (RE= rare earth elements, such as Nd, La) ternary alloys and $Mg_{85}Ni_{15}$ binary alloys. It is interesting to see that the alloys can be activated by hydrogenation and dehydrogenation at 300 °C for 3 and 5 cycles, respectively. For an as-quenched $Mg_{80}Ni_{10}Y_{10}$ alloy, 3

cycles of hydrogen sorption and desorption at 350~385 °C and 30 bar H_2 pressure is necessary for activation of the alloy [31, 32].

2.3.4 Catalyst

The catalytic effect of various elements, including transition metals and their oxides, RE elements, etc (like Nd and La mentioned above), has been reported in many studies. Among all the metal oxides, Nb_2O_5 was identified by Barkhodian et. al. [33] as the most promising catalyst for Mg and Mg based alloys. With 0.2 mol.% Nb_2O_5 added and ball milled for 100 hour, the MgH_2 composite completed full hydrogen desorption in 90 s at 300 °C under vacuum. After desorption, it absorbed about 7 wt.% hydrogen in 1 min at 300 °C under 8.4 bar of hydrogen [34, 35]. Hanada et. al. investigated the hydrogen sorption kinetics of MgH_2 composites ball milled with 1 mol.% Nb_2O_5 for 1 hour. As a result, after 8 hours of dehydrogenation, the catalysed MgH_2 absorbed about 4.5 wt.% hydrogen within 15 s and finally absorbed more than 5 wt.% at room temperature under 10 bar. At 150 and 200 °C, 5 wt.% hydrogen were absorbed within 30 s, then finally up to 5.7 wt.%. Moreover, the product after rehydrogenation treatment released about 6 wt.% hydrogen within 100 min at 160 °C. In their previous work, they also investigated the catalytic effect of Nb_2O_5 using X-ray absorption fine-structure (XAFS) measurement to examine the chemical bonding state. It showed the Nb_2O_5 on the surface of the MgH_2 powder

was reduced during milling, leading to the formation of niobium with a valence less than 5+, as enhanced catalytic activity [34].

3. Experimental methods

3.1 Materials preparation

Mg powders (~40 μm, 99.8 % purity, provided by Alpha Aesar) and Ni powders (<150 μm, 99.99 % purity, provided by Sigma-Aldrich) were used to synthesize $Mg_{90}Ni_{10}$ alloy samples. The powders corresponding to Mg/Ni atomic ratio of 9:1 were mixed together using a mechanical blender (STR4, Stuart Bibby Scientific) for 30 min, followed by isostatic pressing under 80~100 bar pressure for 10 min (Strong-Arm press, Clarke). The compacted Mg-Ni alloy rods were then ready to be loaded for the melt-spinning experiments.

It should be pointed out that the isostatic press technique was employed before melt-spinning in order to avoid any Mg loss, and thus $Mg_{90}Ni_{10}$ alloy samples with less deviation in composition could be synthesised. Since the melting point of Mg (650 °C) is much lower than that of Ni (1455 °C), and the vapour pressure of Mg is roughly 10 times higher than Ni [36], severe loss of Mg can be expected if the raw Mg and Ni powders were melted at the same time during melting-spinning. Therefore, the mechanically alloyed Mg-Ni rods were prepared for the melt-spinning experiments.

3.2 Materials synthesis

An Edmund Buelher D-723729 Hechingen melt spinner (Fig. 1) was used to synthesise the $Mg_{90}Ni_{10}$ alloy samples. The compacted Mg-Ni alloy rods were placed in boron nitride crucible and loaded through the sample port. The melt spinning chamber was flushed 3 times with Ar (partial pressure ~1 bar), and then evacuated until the partial pressure of Ar reached 0.8 bar to provide 0.2 bar pressure for injection. The samples in the crucible were heated to ~600 °C for melting, and the liquid was injected onto a spinning copper wheel to synthesise the melt-spun ribbons. The spacing between the nozzle and the wheel was set up to 0.3 mm, and the rotational speed of the wheel was 2400 rpm (equivalent to a surface velocity of 25 m/s).

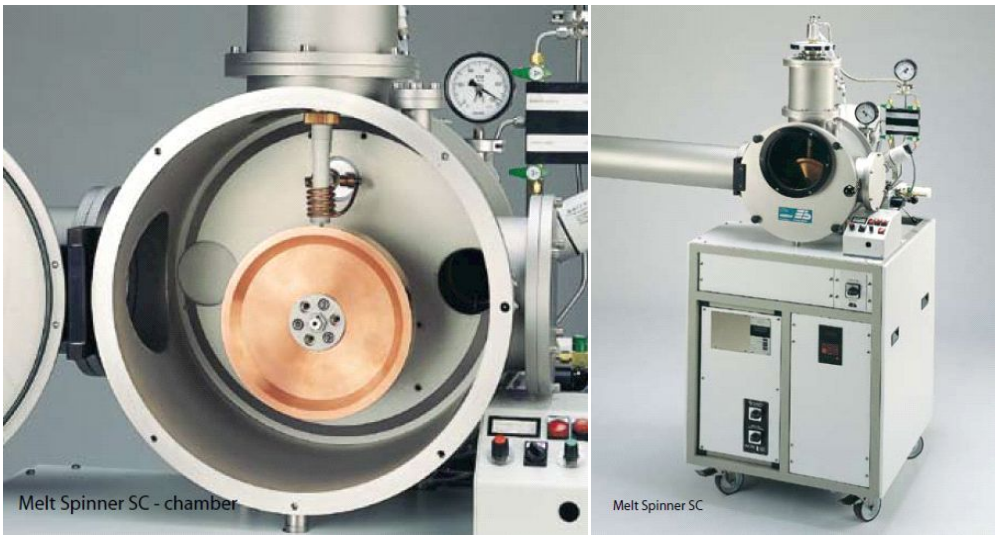

Fig. 1: Image of melt spinner and its chamber.

The melt-spun ribbons were collected and split up into two groups – one for microstructural characterisation and the other to be milled for hydrogen sorption investigations. Freezer milling (SPEX Sample Prep Freezer Mill) was used to grind the melt-spun ribbons. The grinding jar was continually cooled with liquid nitrogen. The time periods for the pre-cooling and milling cycles were both set to 5 min. In total, 3 cycles of milling were carried out, with a 3 min time gap between two cycles. The milled powders were collected in a glove box for hydrogen sorption experiments. For some samples, Nb_2O_5 powder (~325 mesh) was added to the ribbons during milling as a catalyst. The effect of the catalyst addition has also been investigated.

3.3 Microstructural characterisation

Three different experimental methods have been used to characterise the microstructure of the melt-spun $Mg_{90}Ni_{10}$ ribbons: scanning electron microscope (SEM) with energy dispersive spectrometry (EDS); differential scanning calorimetry (DSC); and X-ray diffraction (XRD).

The melt-spun ribbons were mounted in Bakelite, followed by grinding and polishing using Buehler MetaServ® Grinder-Polisher. In the final stage, a polishing diamond suspension (with a diameter of 0.25 μm) was used. The

composition and homogeneity of the polished samples were analysed using a JEOL 6060 SEM.

About 5-15 mg ribbon samples were placed in an alumina crucible, and loaded with an empty crucible for reference in a Netzsch 204HP DSC. Argon flow was applied to protect samples from oxidation. The samples were heated to 450 °C and immediately cooled down to room temperature at 2 °C/min to examine any possible phase transformation.

The melt-spun ribbons were also analysed qualitatively using a Bruker D8 Advanced Diffractometer using CuKα radiation (λ=1.54056Å) at room temperature. The PDF-2 database by ICDD was used to identify any crystal phase forming during melt spinning, i.e., intermetallic compound formation.

3.4 Hydrogen sorption measurements

Constant-temperature thermogravimetric analysis, with a Hiden Intelligent Gravimetric Analyser (IGA) system, was used to investigate the hydrogen sorption capability and kinetics of the melt-spun alloys. Approximately 100 mg samples were loaded in a stainless steel holder in an Ar protection environment. During the hydriding process, 10 bar H_2 gas was flowing through the chamber at 100 ml/min rate. The dehydriding process was conducted under a high vacuum

(~10^{-6} bar). A series of temperatures were chosen for the measurements: room temperature, 140 °C, and 300 °C, with a 5 °C /min heating rate. The weight change of the samples was measured by a microbalance hooked to the sample holder, representing sorption/desorption of the hydrogen.

4. Results

In the present work, melt-spun $Mg_{90}Ni_{10}$ samples were prepared, and it was clear that ribbon-shape products were obtained. Since a high weight loss of Mg was expected during induction melting, the samples were analysed using a SEM with EDS to check the composition, as well as the homogeneity. It is possible to form amorphous phases by melt-spinning, and thus the crystal structures of the phases in the samples was assessed by XRD. In addition DSC was used to measure any phase transformation occurring during the heating and cooling processes, under either Ar or H_2. Finally the H_2 storage properties of the melt-spun $Mg_{90}Ni_{10}$ samples – with and without a catalyst (Nb_2O_5) – was assessed using IGA measurements.

4.1 SEM and EDS results

A secondary electron image of a $Mg_{90}Ni_{10}$ sample is shown in Fig. 2. It can be seen clearly, as expected, that ribbon-shaped materials have been produced using the melt-spinning technique.

The back-scattered electron images of $Mg_{90}Ni_{10}$ sample coated with carbon and gold are shown in Figs. 3 and 4, respectively. In the BSE image of the carbon-coated sample, no obvious contrast is observed, except some white spots which are dirt also seen on the mounting. However, in the BSE image of

the gold-coated sample, white and grey contrast in the ribbon matrix can be seen clearly, as well as some black regions which are holes. The compositions of different areas on the samples, were determined by EDS and are listed in Table 1.

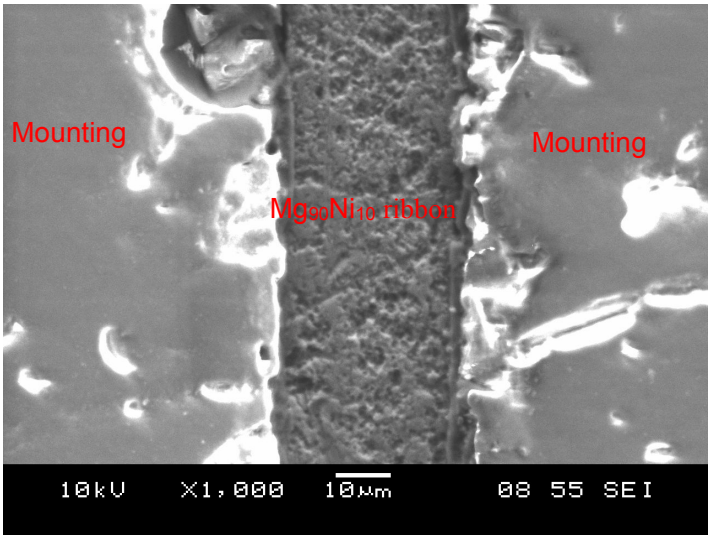

Fig. 2: Secondary electron image of melt-spun $Mg_{90}Ni_{10}$ ribbon.

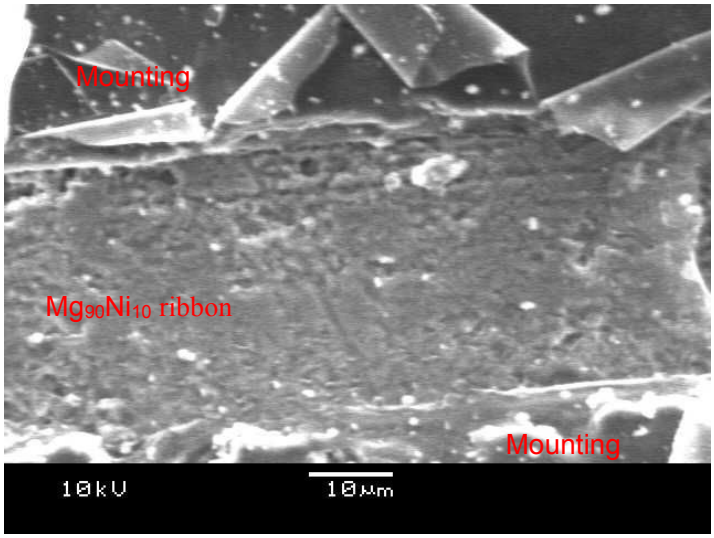

Fig. 3: Back-scattered electron image of $Mg_{90}Ni_{10}$ sample coated with carbon.

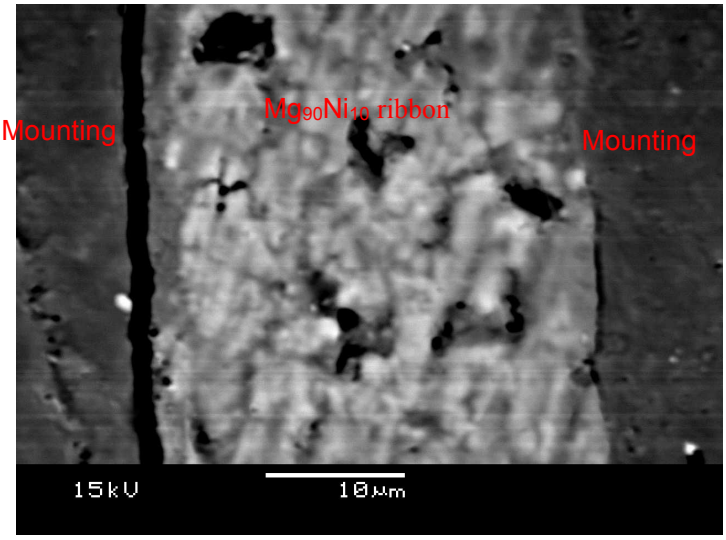

Fig. 4: Back-scattered electron image of melt-spun $Mg_{90}Ni_{10}$ ribbon coated with gold.

Table 1: The compositions of $Mg_{90}Ni_{10}$ sample determined by EDS.

Spectrum No.	Mg at.%	Ni at.%
1	89.5 (+/- 0.3)	10.5 (+/- 0.3)
2	88.2 (+/- 0.1)	11.8 (+/- 0.2)
3	87.4 (+/- 0.1)	12.6 (+/- 0.3)
4	88.7 (+/- 0.2)	11.3 (+/- 0.3)
5	86.7 (+/- 0.2)	13.3 (+/- 0.4)
6	90.0 (+/- 0.2)	10.0 (+/- 0.2)
7	88.9 (+/- 0.1)	11.1 (+/- 0.1)
8	87.2 (+/- 0.3)	12.8 (+/- 0.2)
9	88.5 (+/- 0.2)	11.5 (+/- 0.2)
10	89.1 (+/- 0.1)	10.9 (+/- 0.1)

4.2 XRD results

X-ray diffraction has been used in order to study the microstructure of the melt-spun $Mg_{90}Ni_{10}$ alloy. An X-ray diffraction pattern for the sample is shown in Fig. 5. Some peaks at low angles have been found representing Mg. A small peak at 37.9° is attributed to a meta-stable phase Mg_6Ni. Intensity of other peaks detected at high angles are weak meaning that the majority of the melt-spun $Mg_{90}Ni_{10}$ sample contains phases which are nanocrystalline or amorphous.

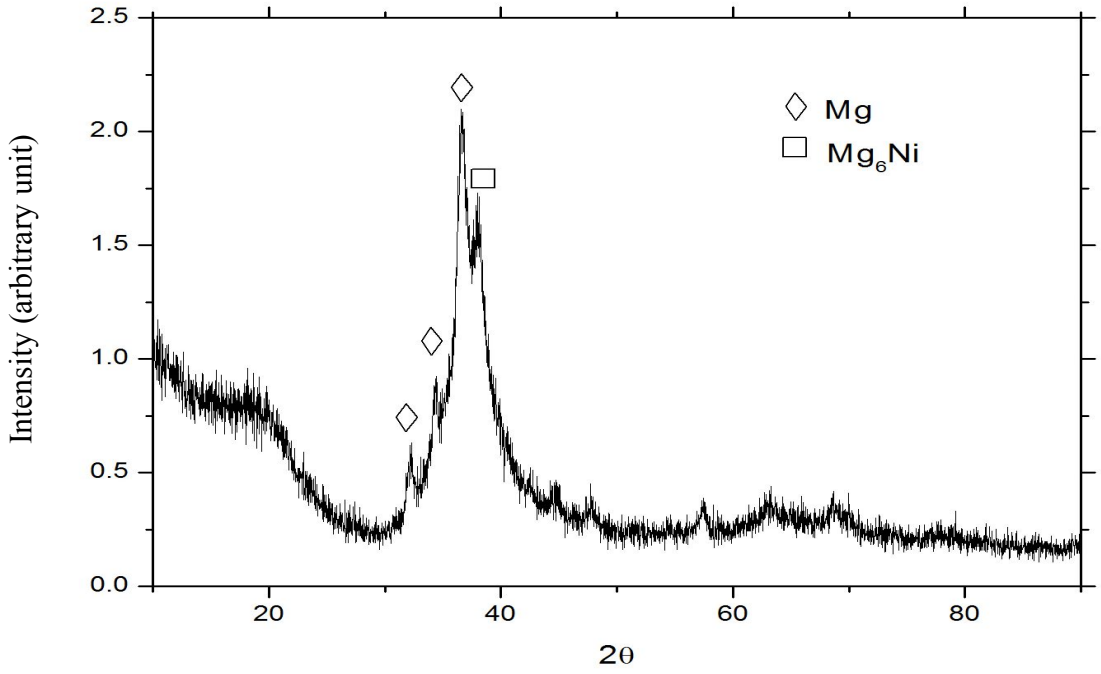

Fig. 5: XRD pattern of a melt-spun $Mg_{90}Ni_{10}$ sample

The IGA measured sample (to be described in the following sub-section) was then analysed by XRD, and the patterns is shown in Fig 6. The following phases

were detected: (Mg), Mg_2Ni, MgH_2, HT-Mg_2NiH_4 (high temperature structure), and LT-Mg_2NiH_4 (low temperature structure).

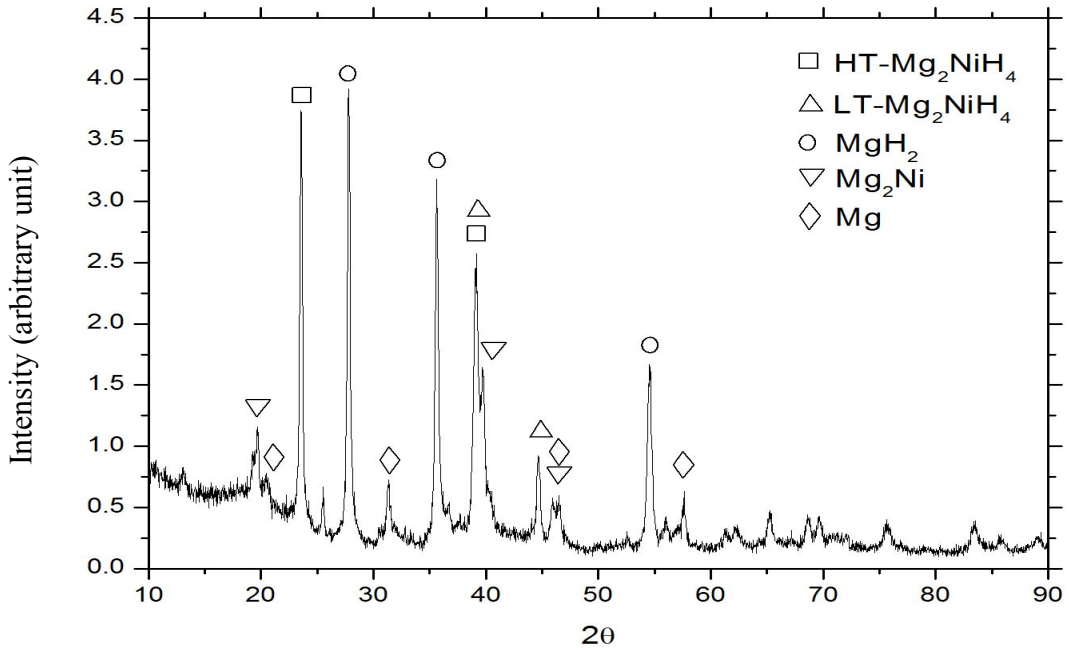

Fig. 6: XRD pattern of melt-spun $Mg_{90}Ni_{10}$ ribbon after being heated under 10 bar H_2.

4.3 DSC results

Differential scanning calorimetry (DSC) was carried out on melt-spun $Mg_{90}Ni_{10}$. Fig. 7 shows the DSC for $Mg_{90}Ni_{10}$ during heating and cooling in 3 bar Ar atmosphere. In the figure, there is an exothermic reaction occurring at 150 °C during heating, with no corresponding peak during cooling. Above 350 °C, an endothermic peak is seen on the heating curve.

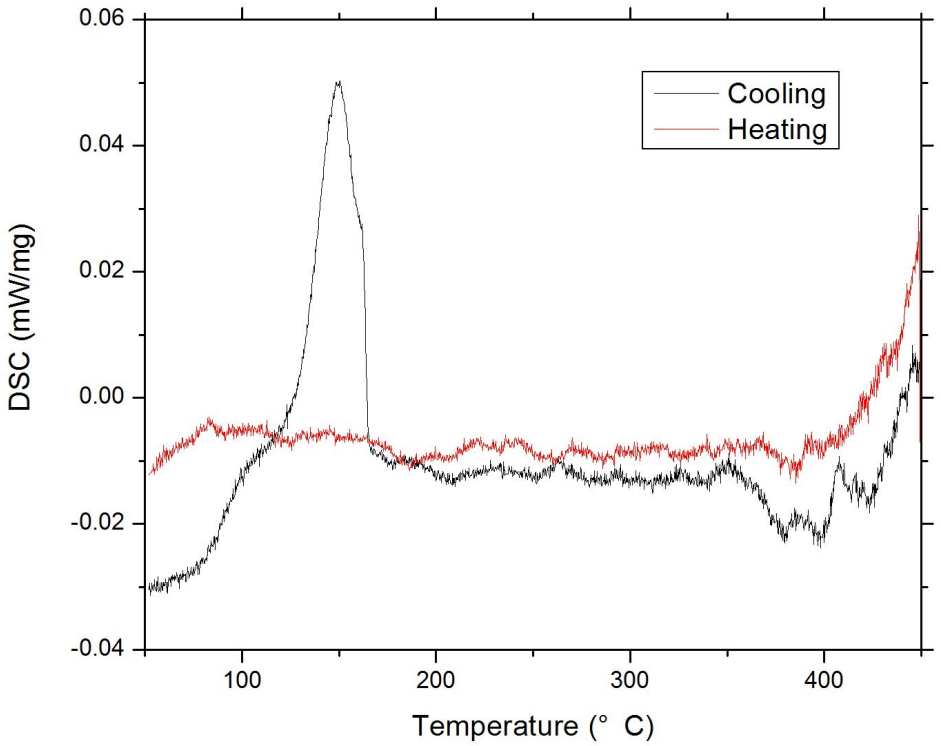

Fig. 7: DSC of melt-spun $Mg_{90}Ni_{10}$ heated and cooled in 3 bar Ar at 2 °C/min.

Fig. 8 shows the DSC of $Mg_{90}Ni_{10}$ during heating and cooling in 10 bar H_2. There is an exothermic peak found at 150 °C during heating, with no corresponding peak during cooling. However, an endothermic peak can be seen clearly at 350 °C during heating, and the corresponding exothermic peak is at 300 °C during cooling.

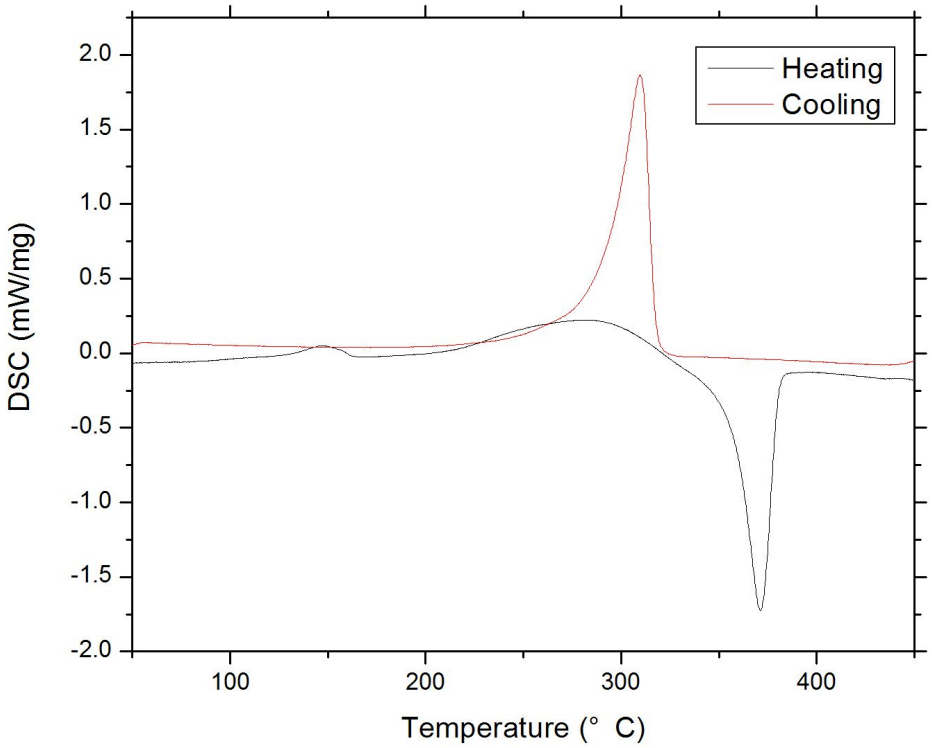

Fig. 8: DSC of melt-spun $Mg_{90}Ni_{10}$ heated and cooled in 10 bar H_2 at 2 °C/min.

DSC for the melt-spun $Mg_{90}Ni_{10}$ ribbon ball-milled with 0.2 mol.% Nb_2O_5 powder, was performed under 3 bar Ar, as shown in Fig. 9. Two heating and cooling runs were carried out for the sample. Both heating curves exhibit three exothermic peaks: at 150 °C, 300 °C and 350 °C.

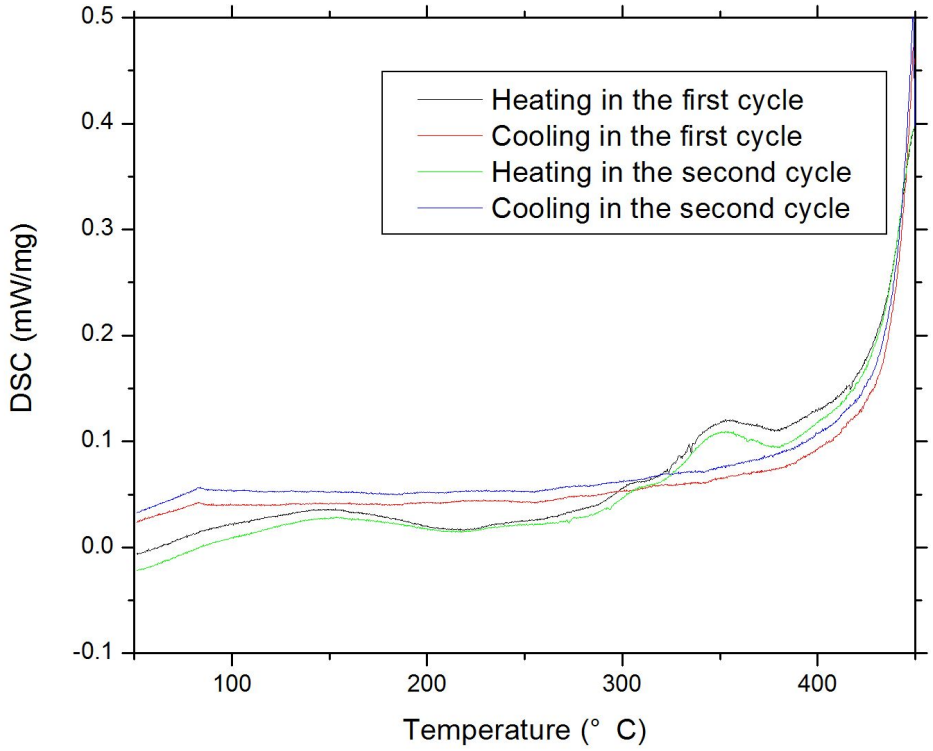

Fig. 9: DSC results of melt-spun $Mg_{90}Ni_{10}$ milled with 0.2 mol.% Nb_2O_5, heated and cooled in 3 bar Ar at 2 °C/min

DSC profiles for two runs of heating and cooling for the melt-spun $Mg_{90}Ni_{10}$ ball-milled with 0.2 mol.% Nb_2O_5 powder, heated in 10 bar H_2, as shown in Fig. 10. The DSC plots are more complicated than the previous plots. During the first heating process, there are exothermic reactions at 150 and 270 °C. An endothermic reaction at 350 °C is found during heating, and a corresponding exothermic peak is observed at 300 °C during cooling. One more endothermic peak can also be seen at 400 °C on the heating curve for the second run, but it is not seen in the first run and no corresponding peak is seen during cooling.

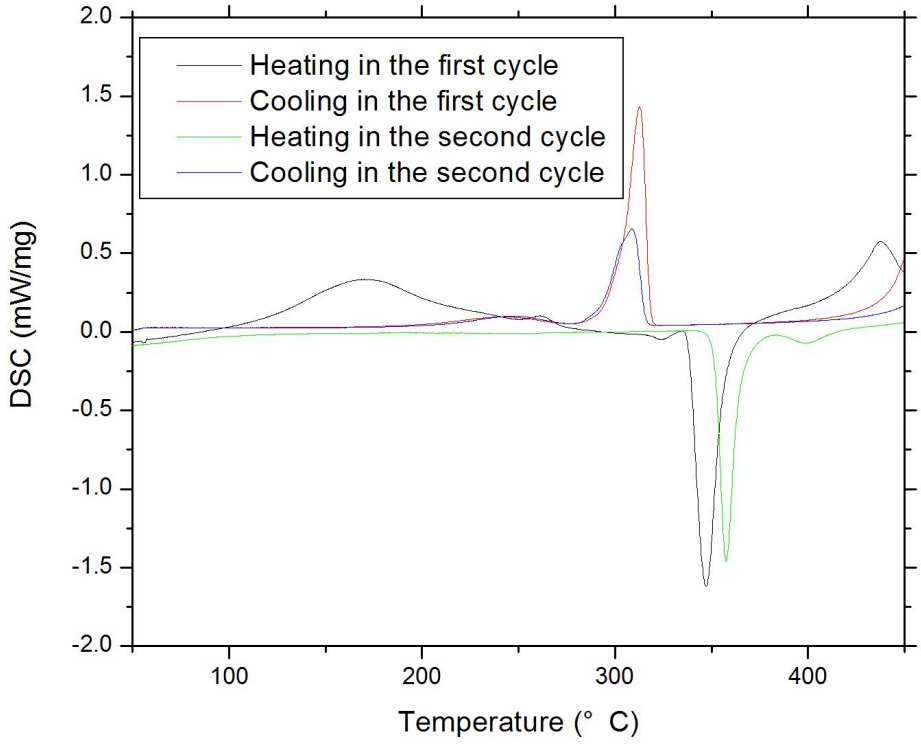

Fig. 10: DSC of melt-spun $Mg_{90}Ni_{10}$ ball-milled with 0.2 mol.% Nb_2O_5 during heating and cooling in 10 bar H_2 at 2 °C/min

4.4 IGA measurements

A series of intelligent gravimetric analyser (IGA) measurements were carried out to analyse the hydrogen sorption behaviour of the melt-spun $Mg_{90}Ni_{10}$ summarised in Table 2. The results are shown in Figs 11 - 19. Note that the results are presented and described separately in this Chapter and the next Chapter.

Table 2: Summary of IGA measurements.

Test No.	Temperature (°C)	Cycle	Catalyst (Nb_2O_5)
1	25 (room temperature)	1 (as activation)	No
2	25 (room temperature)	2	No
3	25 (room temperature)	1	Yes
4	140	1 (as activation)	No
5	140	2	No
6	140	1	Yes
7	300	1 (as activation)	No
8	300	2	No
9	300	1	Yes

Figs. 11 and 12 show the hydrogen uptake of melt-spun $Mg_{90}Ni_{10}$ at room temperature during the first and second cycle, respectively. The weight percent of hydrogen increased up to 0.16% after 8000 s in 10 bar hydrogen. While during the second cycle, the hydrogen uptake has increased above 2% within 8000s.

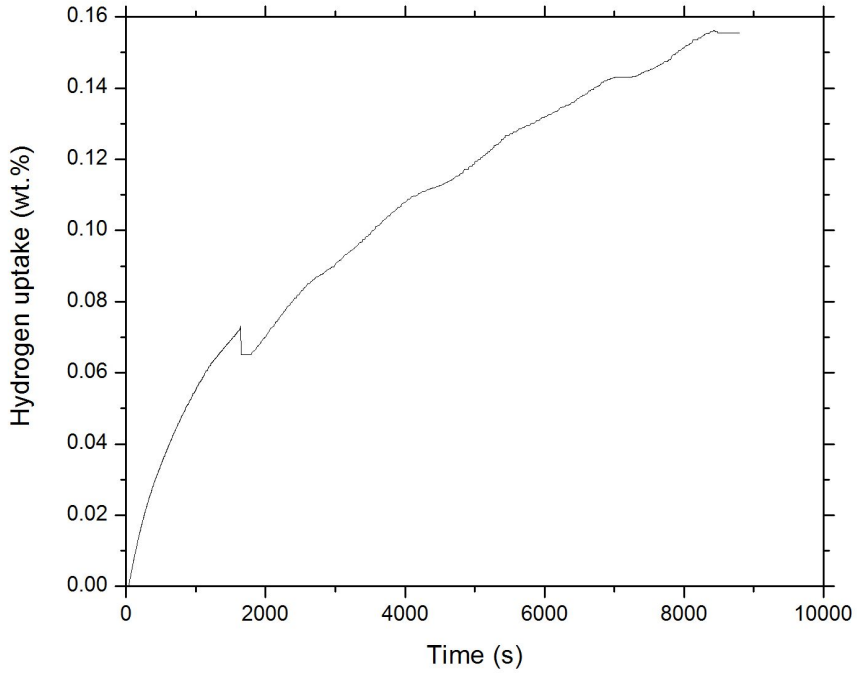

Fig. 11: IGA showing H_2 uptake of melt-spun $Mg_{90}Ni_{10}$ at room temperature under 10 bar H_2.

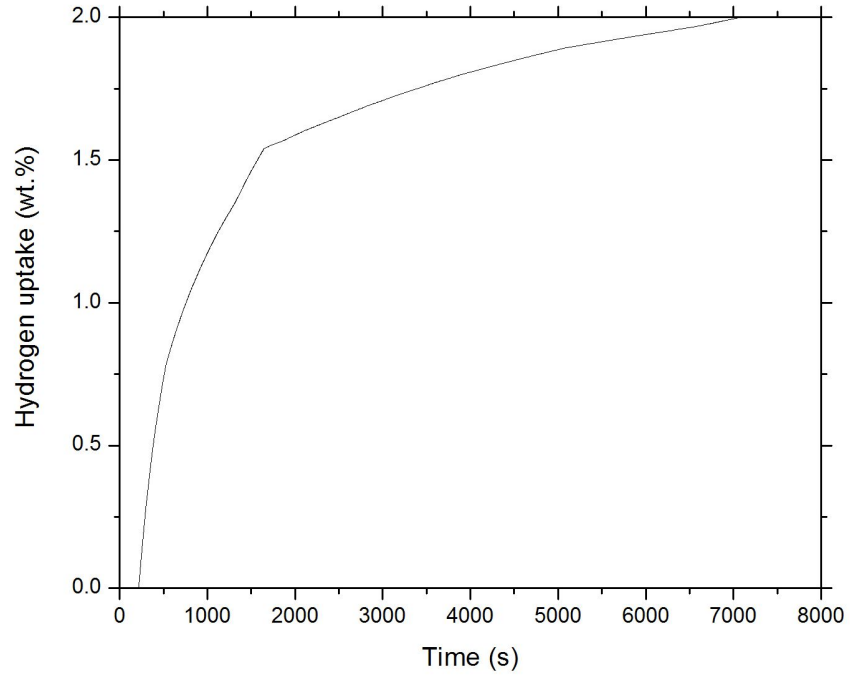

Fig. 12: IGA showing H_2 uptake of melt-spun $Mg_{90}Ni_{10}$ after having been run once (Fig. 11), at room temperature.

When the temperature increases to 140 °C, the hydrogen uptake for melt-spun $Mg_{90}Ni_{10}$ is shown in Figs. 13 and 14 for the first and second cycles, respectively. After 3000 s the hydrogen sorption capability reaches 1.2 wt.% for the first cycle, and then increases to almost 4 wt.% during the second cycle.

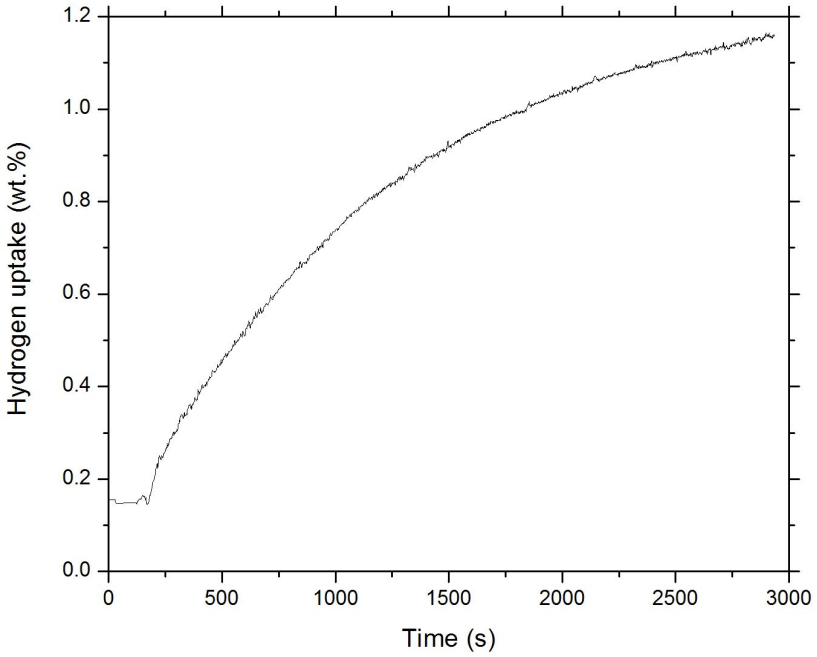

Fig. 13: IGA showing the H_2 uptake of melt-spun $Mg_{90}Ni_{10}$ at 140 °C in 10 bar H_2.

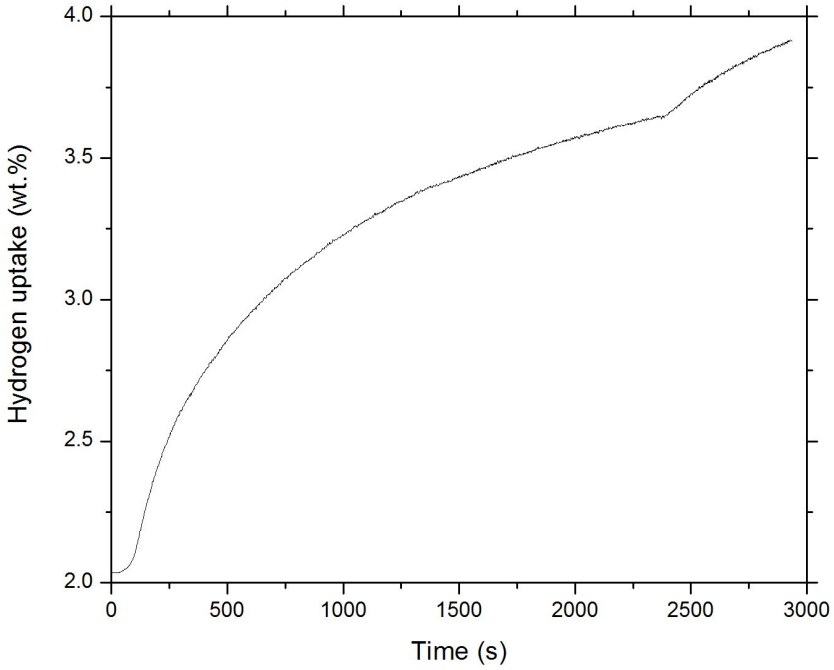

Fig. 14: IGA showing H_2 uptake of melt-spun $Mg_{90}Ni_{10}$ at 140 °C in 10 bar H_2 during the second cycle.

The hydrogen sorption measurements were also performed at 300 °C, the results of which during two cycles are shown in Figs. 15 and 16. It is interesting to see an inflection point at around 9000 s, when the hydrogen uptake has abruptly increased from 0.18 wt.% to 1.18 wt.% within 3000 s. Moreover, hydrogen sorption during the second cycle can reach 4 wt.% at the start of the measurement.

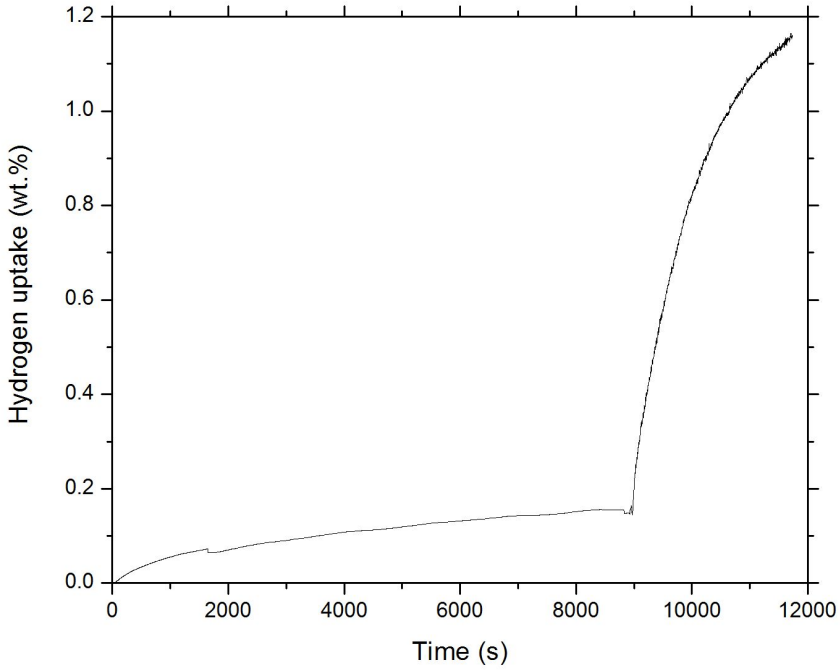

Fig. 15: IGA showing H_2 uptake of melt-spun $Mg_{90}Ni_{10}$ at 300 °C in 10 bar H_2.

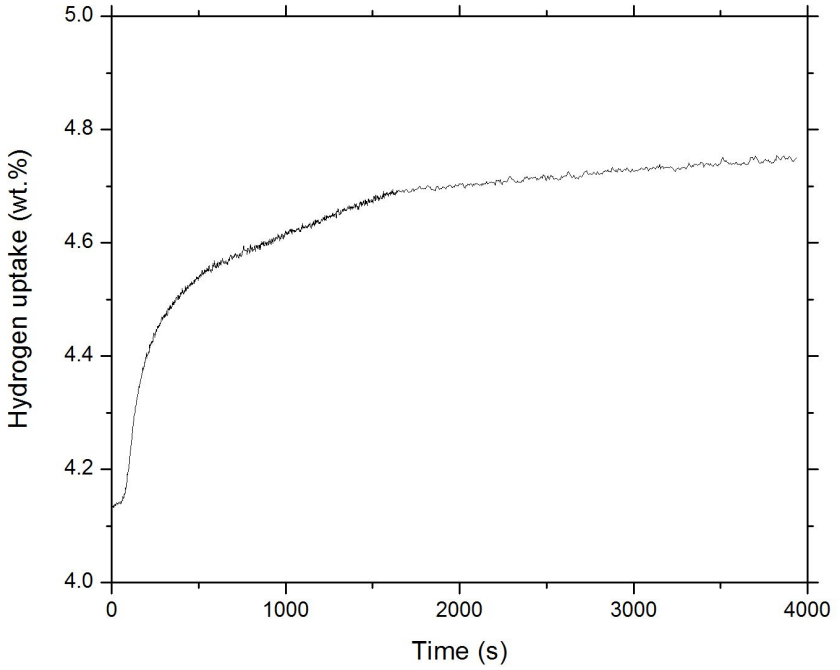

Fig. 16: IGA showing H_2 uptake of melt-spun $Mg_{90}Ni_{10}$ at 300°C in 10 bar H_2, during the second cycle.

The IGA measurements for melt-spun $Mg_{90}Ni_{10}$ ball-milled with 0.2 mol.% Nb_2O_5, at room temperature, 140 °C and 300 °C, are shown in Figs. 17 - 19. Within 8000 s at room temperature the hydrogen uptake has increased to above 2.8 wt.%. However, this value is only about 1.6 wt.% at 140 °C. When the temperature rises to 300 °C, the inflection point is found to be 50 s, too early a stage and the test was aborted.

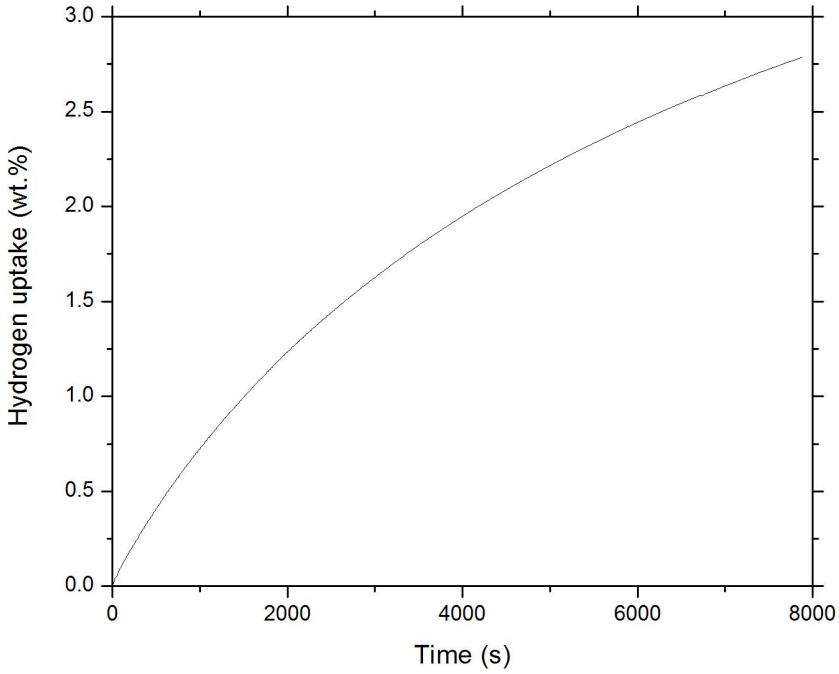

Fig. 17: IGA showing H_2 uptake of melt-spun $Mg_{90}Ni_{10}$ ball-milled with 0.2 mol.% Nb_2O_5, in 10 bar H_2 at room temperature.

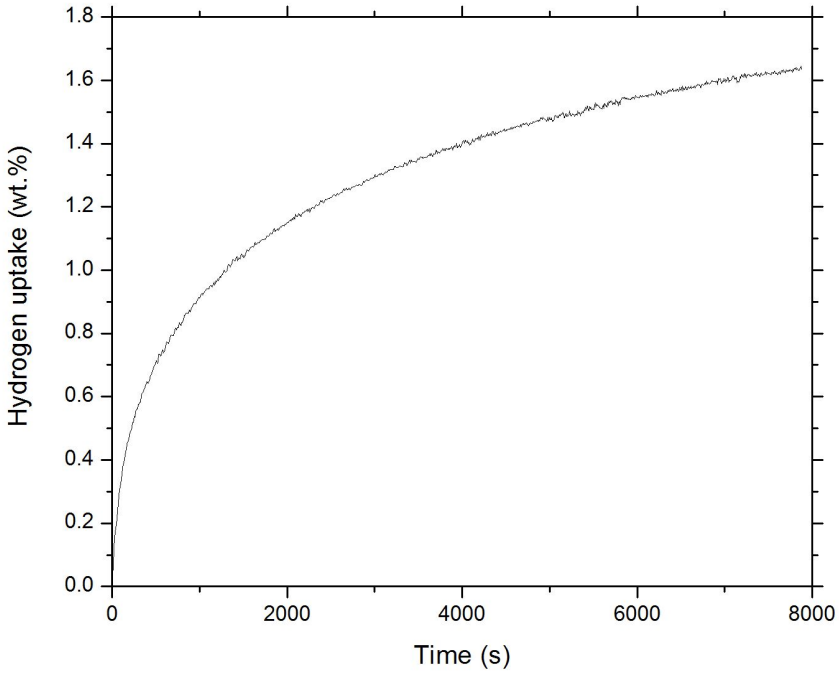

Fig. 18: IGA showing H_2 uptake of melt-spun $Mg_{90}Ni_{10}$ ball-milled with 0.2 mol.% Nb_2O_5, in 10 bar H_2 at 140°C.

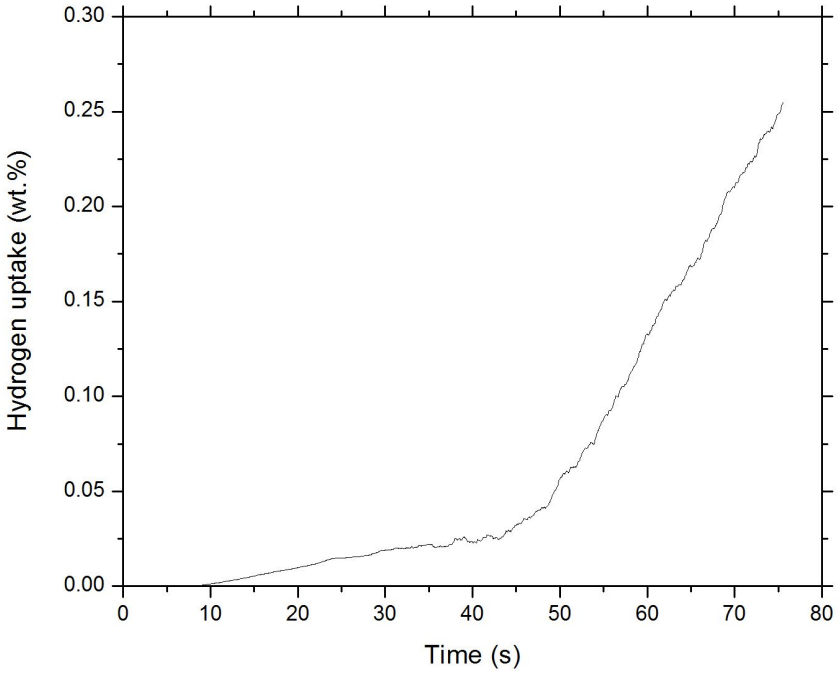

Fig. 19: IGA showing H_2 uptake of melt-spun $Mg_{90}Ni_{10}$ ball-milled with 0.2 mol.% Nb_2O_5, in 10 bar H_2 at 300°C.

5. Discussion

5.1 Composition of the melt-spun ribbons

One of the most important purposes for using melt-spun technique for the $Mg_{90}Ni_{10}$ alloy synthesis is to produce homogenous ribbon samples. From the secondary electron image in Fig. 2 it is easy to see that the sample synthesis of ribbon- shape has been successful.

Moreover, there is no significant contrast within the matrix in the back-scattered electron images in Figs. 3 and 4, which means that the composition is relatively homogenous in the synthesised ribbons. However, some precipitates can also be seen clearly within the matrix. The EDS results in Table 1 also indicate the homogeneity of the composition. In addition the obtained composition is slightly higher in Ni due to Mg loss during induction melting, but the deviation from the mean composition is not great.

5.2 Microstructure of the melt-spun ribbons

Since it is known that a nanocrystalline or amorphous microstructure can improve the hydrogen sorption speed [3], it is of interest to try to synthesize $Mg_{90}Ni_{10}$ ribbons with such a microstructure. The exothermic peaks during heating in the DSC (Figs. 7 - 10) all indicate the recrystallisation of an

amorphous phase, as no corresponding endothermic peak is observed during cooling.

To confirm the presence of an amorphous phase in the melt-spun ribbons, XRD was performed. The broad low angle peak in Fig. 5 suggests the majority of the sample contains an amorphous and/or nanocrystalline phase(s).

5.3 Hydrogen sorption

For room temperature, 140 °C, and 300 °C the comparison of the hydrogen sorption performance during the first and second cycles is shown in Figs. 20 - 22, respectively. In all the three figures, the hydrogen uptakes during the second cycle were much higher than that during the first cycle, indicating that the activation process can have a significant effect on the hydrogen absorption. In addition the hydrogen uptake curves after activation at different temperatures are compared in Fig. 23. It is shown that the hydrogen sorption capacity increases as the temperature increases.

In addition, the hydrogen uptake difference between the first and second cycles intends to be smaller when temperature rises from 25 to 300 °C. This means that the activation effect has been weakened after heating to a higher temperature.

According to recent work by Yi [37], the optimum activation treatment temperature depends on the alloy composition and the synthesis method.

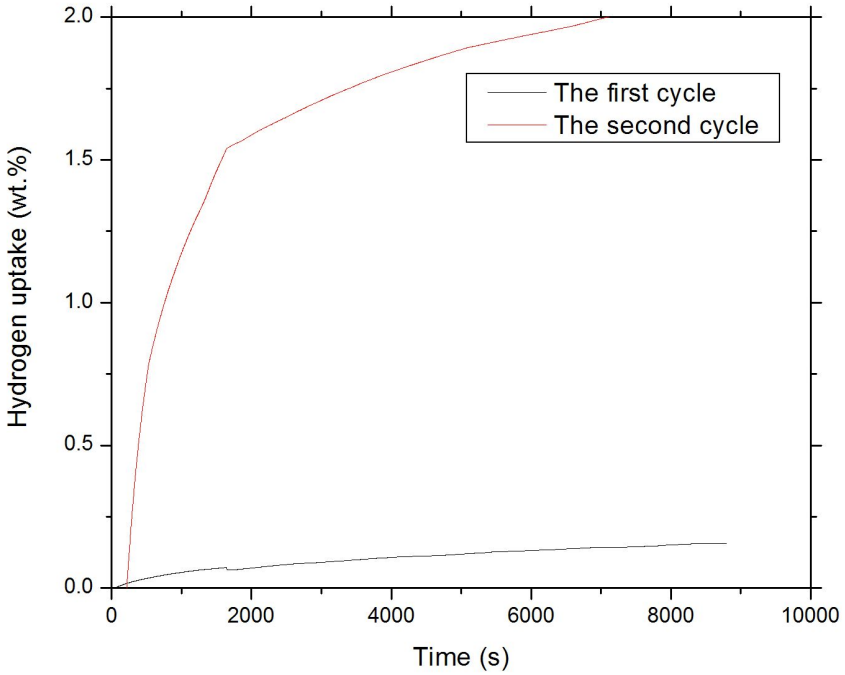

Fig. 20: IGA showing H_2 absorption of melt-spun $Mg_{90}Ni_{10}$ in 10 bar H_2 during the first and second cycle at room temperature.

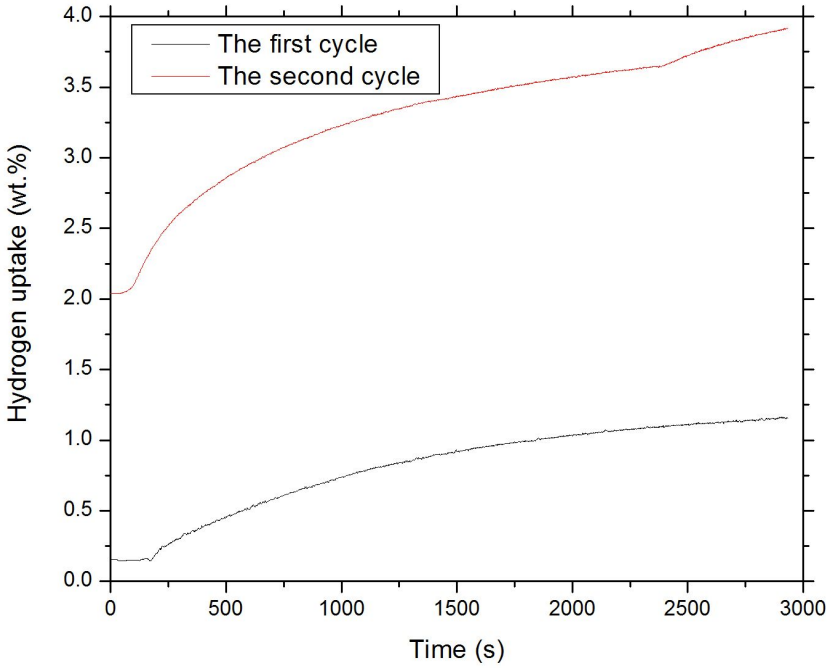

Fig. 21: IGA showing H_2 absorption of melt-spun $Mg_{90}Ni_{10}$ in 10 bar H_2 during the first and second cycle at 140 °C.

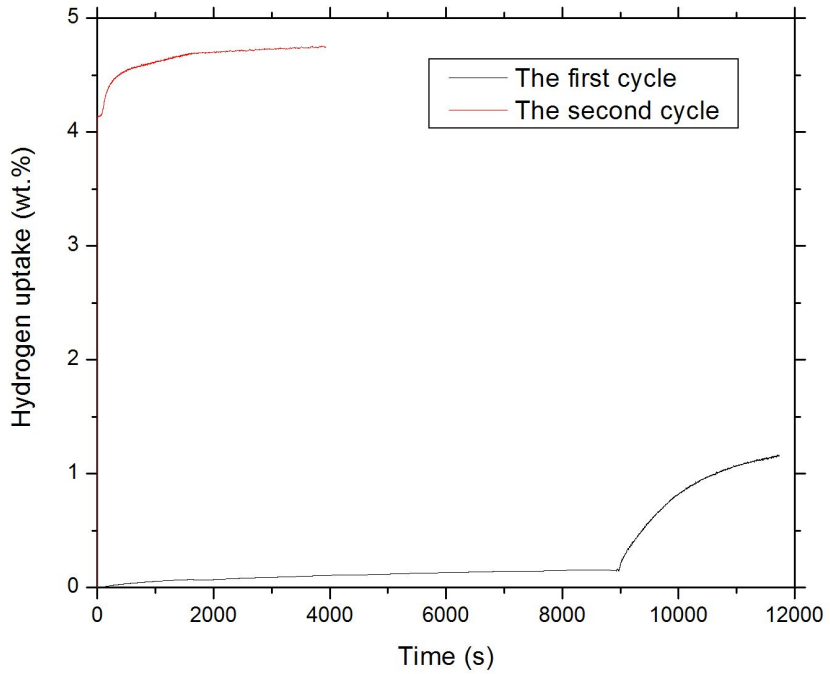

Fig. 22: IGA showing H_2 absorption of melt-spun $Mg_{90}Ni_{10}$ in 10 bar H_2 during the first and second cycle at 300 °C.

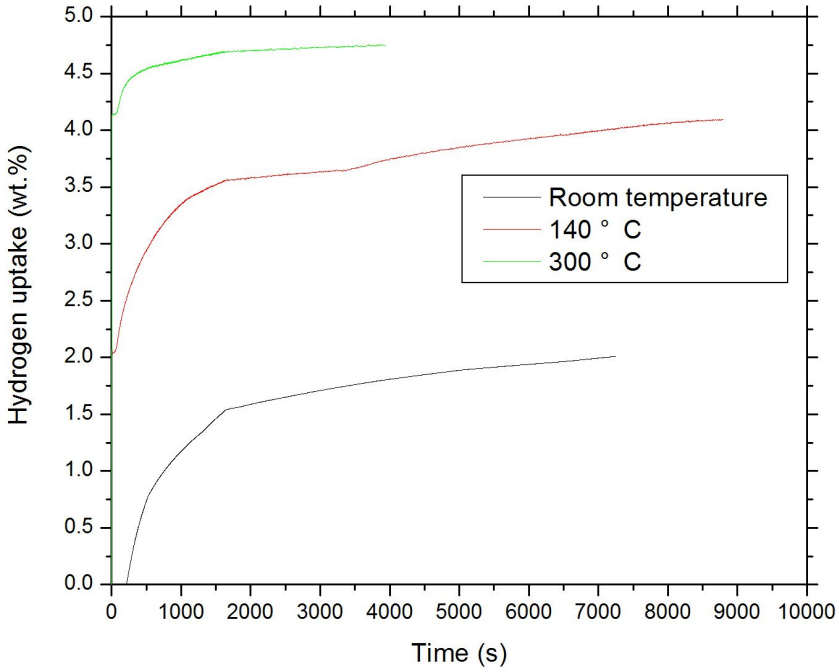

Fig. 23: IGA showing H_2 absorption of melt-spun $Mg_{90}Ni_{10}$ in 10 bar H_2 after activation treatment at room temperature, 140 °C, and 300 °C.

Comparison of the hydrogen sorption properties at different temperatures of un-catalysed melt-spun $Mg_{90}Ni_{10}$ versus melt-spun $Mg_{90}Ni_{10}$ ball-milled with a catalysis (0.2 mol.% Nb_2O_5) is shown in Figs. 24 - 26. The effect of the addition of the Nb_2O_5 powder is a very significant improvement in the hydrogen sorption properties. However, this effect is not so pronounced when at higher temperatures.

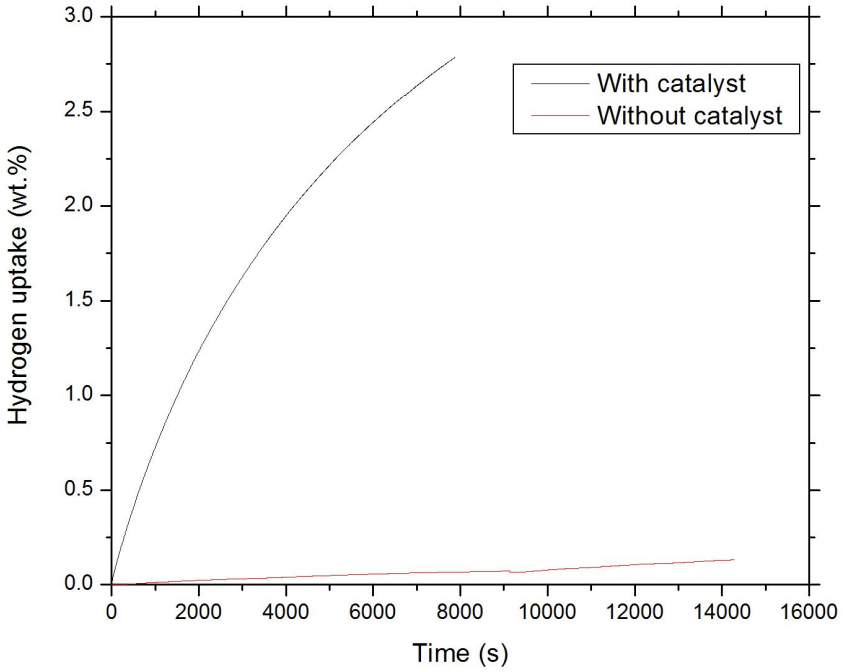

Fig. 24: IGA showing H_2 absorption of melt-spun $Mg_{90}Ni_{10}$ with and without a catalyst (0.2 mol.% Nb_2O_5) in 10 bar H_2 at room temperature.

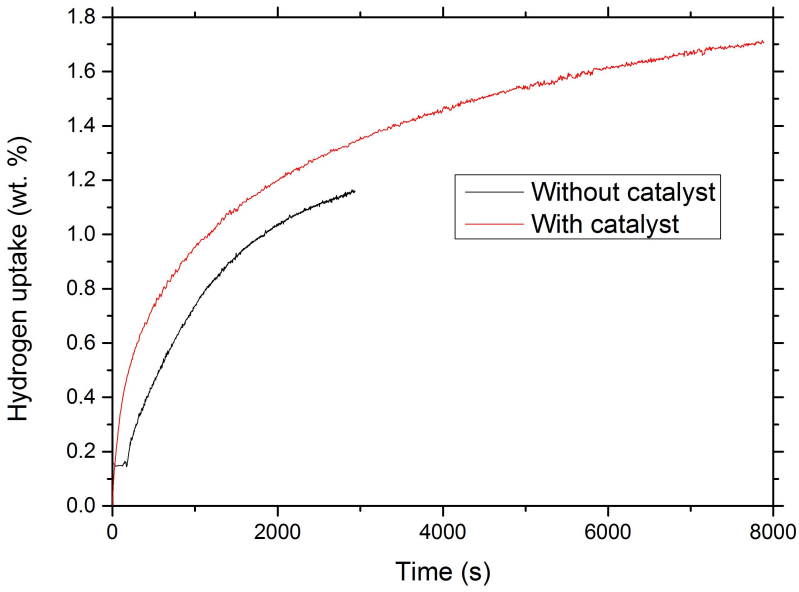

Fig. 25: IGA showing H_2 absorption of melt-spun $Mg_{90}Ni_{10}$ with and without a catalyst (0.2 mol.% Nb_2O_5) in 10 bar H_2 at 140°C.

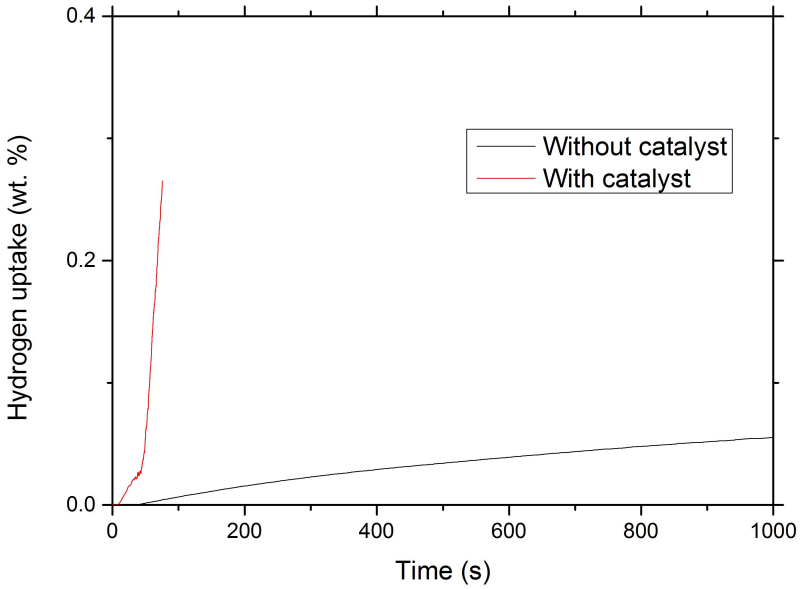

Fig. 26: IGA showing H_2 absorption of melt-spun $Mg_{90}Ni_{10}$ with and without a catalyst (0.2 mol.% Nb_2O_5) in 10 bar H_2 at 300°C.

5.4 Mechanism of hydrogen sorption

Although the hydrogen sorption performance of the $Mg_{90}Ni_{10}$ ribbons have been reported in the previous sections, it is also important to understand the mechanism of hydrogen absorption and desorption. The peaks in the DSC curves in Fig. 8 have been labelled as shown in Fig. 27. Without a catalyst, only one reaction occurs during hydrogen absorption and desorption. This is very likely to be: $Mg + H_2 \Leftrightarrow MgH_2$. Similar peaks have recently been reported by Li [38].

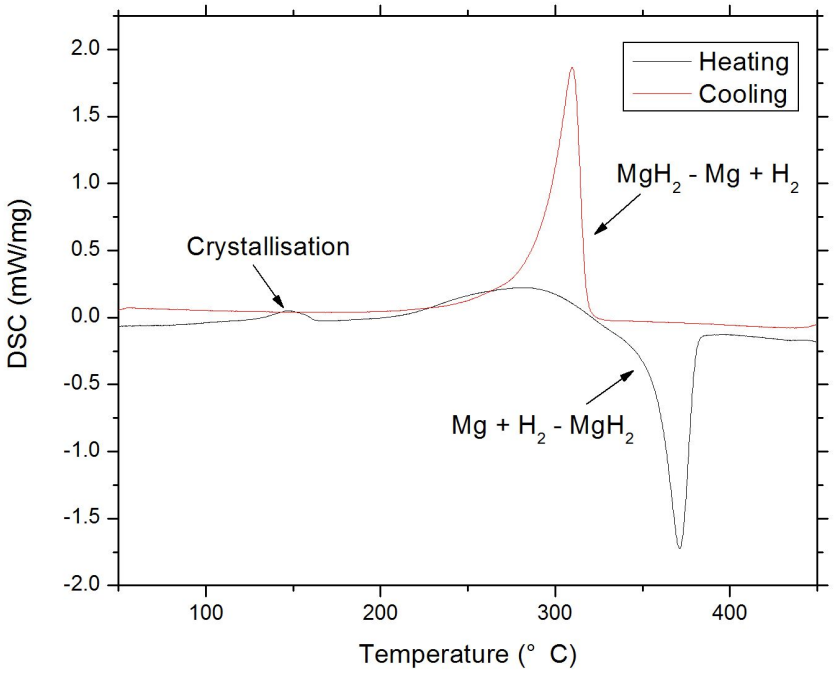

Fig. 27: DSC of melt-spun $Mg_{90}Ni_{10}$ heated and cooled in 10 bar H_2 at 2 °C/min (labelled version of Fig. 8)

The DSC plots are more complicated when a Nb_2O_5 catalyst has been added and ball-milled with the $Mg_{90}Ni_{10}$ ribbons, as shown in Fig. 28. The large peaks representing the reaction ($Mg + H_2 \Leftrightarrow MgH_2$) are again observed. The onset and offset temperatures of hydrogen sorption during heating are 340 °C and 380 °C, respectively. For hydrogen desorption during cooling, the onset and offset temperatures are about 320 °C and 290 °C, respectively. A MgH_2 phase has also been determined in the sample after IGA test using XRD as shown in Fig. 6.

During the first heating cycle a small peak with an onset temperature of about 330 °C is observed in Fig. 28, which is not observed for the sample without a catalyst shown in Fig. 27. This peak has been attributed to the reaction of $Mg_2Ni + 2H_2 \Leftrightarrow Mg_2NiH_4$ [38], since Mg_2Ni has also formed during the first heating represented by the small exothermic peak at about 250 °C. However the peak corresponding to the same reaction has shifted to a higher temperature in the second heating cycle. This shift implies that the reaction requires higher activation energy as its driving force during latter cycles. The reason for this phenomenon can be explained as follows.

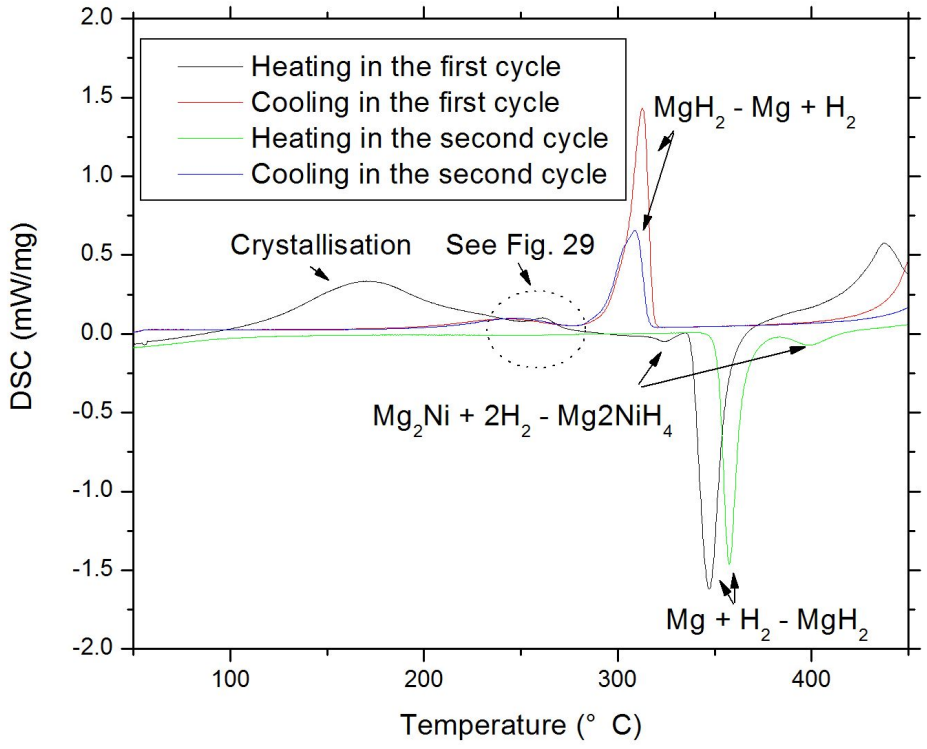

Fig. 28: DSC of melt-spun $Mg_{90}Ni_{10}$ ball-milled with 0.2 mol.% Nb_2O_5, during heating and cooling in H_2 at 2 °C/min (labelled version of Fig. 10).

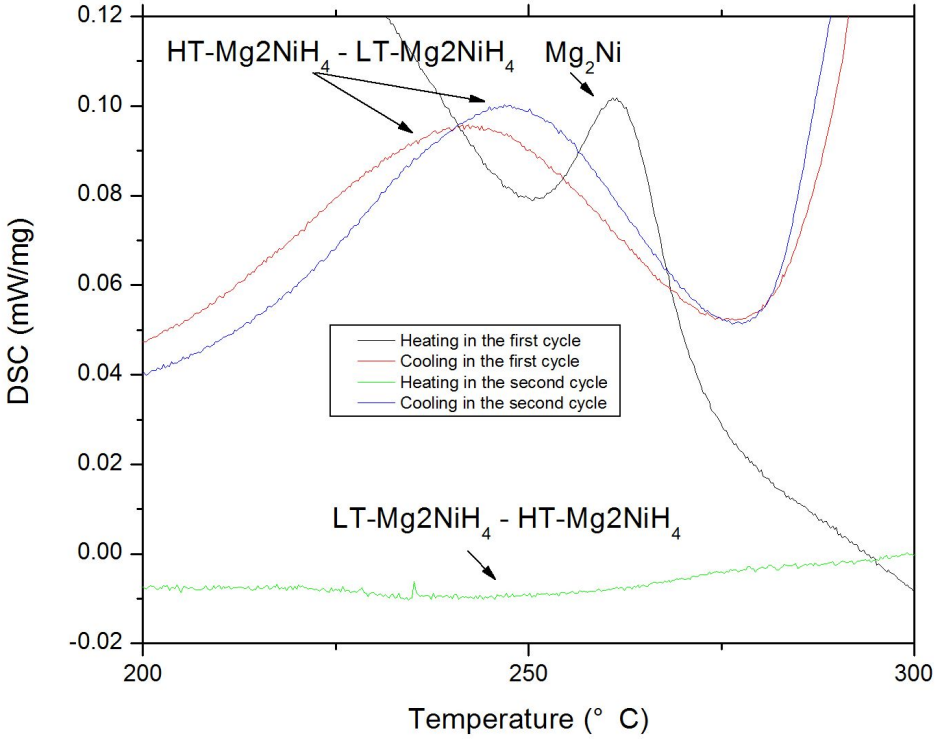

Fig. 29: Magnified region of the dotted circle in Fig. 28.

Considering that no obvious peak representing the decomposition of Mg_2NiH_4 has been found during cooling, the reaction kinetics of decomposition of Mg_2NiH_4 must be much slower than that of its formation. However, the residual Mg_2NiH_4 phase transforms to another allotropic structure at around 200 – 220 °C (HT- Mg_2NiH_4 ⇔ LT- Mg_2NiH_4) [31, 38]. Although it is a reversible reaction, less Mg_2NiH_4 with low temperature structure has transformed back to the high temperature structure, since the representative peak on the second heating curve (not seen on the first heating curve) is so small. This is also confirmed by the XRD results in Fig. 6, showing that both HT-Mg_2NiH_4 and LT-Mg_2NiH_4 phases have been retained after the IGA measurement. Therefore, the residual Mg_2NiH_4

phase has hindered the further formation of Mg_2NiH_4, and thus a higher activation energy or driving force is essential. This eventually leads to a shift in the formation peak for the Mg_2NiH_4 phase to a higher temperature in the second cycle.

6. Summary

Melt-spun $Mg_{90}Ni_{10}$ ribbon has been synthesised in the present work. SEM analysis has shown that the composition of the alloy matrix is fairly homogeneous, with at present some precipitates. XRD and DSC results show that an amorphous phase is produced within the melt-spun sample. IGA measurements in 10 bar hydrogen have shown that the higher the temperature, the larger the hydrogen uptake. In addition one sorption/desorption cycle is required in order to activate the materials and thereby increase significantly the hydrogen uptake capacity.

Two types of magnesium hydrides were found to form during the reactions with hydrogen: MgH_2 and Mg_2NiH_4. The mechanism of hydrogen sorption/desorption has been explained based on a series of DSC, XRD and IGA measurements. Moreover, Nb_2O_5 has been shown to be an efficient catalyst for hydrogen sorption in melt-spun Mg-Ni ribbons.

Some future experiments are recommended to be carried out. In-situ XRD measurements are important to identify the hydrides formed at high temperatures during the absorption process. In addition it would be interesting to determine probably with a synchrotron how much HT-Mg_2NiH_4 has transformed

to LT-Mg_2NiH_4 during cooling, and how much this is affecting hydrogen sorption during subsequent cycles.

References

[1] M. Hirscher, Handbook of hydrogen storage, WILEY-VCH, Weinheim (2010).

[2] R.A. Varin, T. Czujko, and Z.S. Wronski, Nanomaterials for solid state hydrogen storage, Springer, New York (2009).

[3] S. Orimo, and H. Fujii, Materials science of Mg-Ni-based new hydrides, Appl. Phys. A, 72, pp. 167-186 (2001).

[4] M.U. Niemann, S.S. Srinivasan, A.R. Phani, A. Kumar, D.G. Goswami, and E.K. Stefanakos, Nanomaterials for hydrogen storage applications: A review, Journal of Nanomaterials, pp. 1-9 (2008).

[5] B. Peng, J. Liang, Z. Tao, and J. Chen, Magnesium nanostructures for energy storage and conversion, J. Mater. Chem., 19, pp. 2877-2883 (2009).

[6] P. Ekins, Hydrogen energy: Economic and social challenges, Earthscan, London (2010).

[7] J. Rifkin, The hydrogen economy: The creation of the world-wide energy web and the redistribution of power on earth, Polity Press, Oxford (2002).

[8] A. Züttel, A. Borgschulte, and L. Schlapbach, Hydrogen as a future energy carrier, WILEY-VCH, Weinheim (2008).

[9] M. Ball, and M. Wietschel, The hydrogen economy: Opportunities and challenges, Cambridge University Press, Cambridge (2009).

[10] L. Schlapbach, and A. Züttel, Hydrogen-storage materials for mobile applications, Nature, 414, pp. 353-358 (2001).

[11] Quantum News: In brief: Quantum looking to transfer H2 storage technology to Japanese automakers, Fuel Cells Bulletin, 6, p.7 (2005).

[12] J.C.F. Wang, and E.C.E. Ronnebro, An overview of hydrogen storage for transportation application, in TMS Annual Meeting 2005, San Francisco, CA, USA, pp. 21-24 (2005).

[13] Department of Energy (DOE), DOE targets for onboard hydrogen storage systems for light-duty vehicles, (2009). Available online: http://www1.eere.energy.gov/hydrogenandfuelcells/storage/pdfs/targets_onboard_hydro_storage.pdf

[14] T. Graham, On the absorption and dialytic separation of gases by colloid septa, Philosophical Transactions of the Royal Society of London, 156, pp. 399-439 (1866).

[15] T.C. Ehlert, R.M. Hilmer, and E.A. Beauchamp, A mass spectrometric study of the vaporization of magnesium, calcium, magnesium hydride and calcium hydride, Journal of Inorganic and Nuclear Chemistry, 30, pp. 3112-3115 (1968).

[16] K.H. Buschow, and H.H. Van Mal, Phase relations and hydrogen absorption in the lanthanum-nickel system, J. Less Com. Met., 29, pp. 203-210 (1972).

[17] J.J. Reilly, and R.H. Wiswall Jr., The reaction of hydrogen with alloys of magnesium and nickel and the formation of Mg_2NiH_4, Inorganic Chemistry, 7, pp. 2254-2256 (1968).

[18] J.-P. Bastide, B. Bonnetot, J.-M. Létoffé, and P. Claudy, Polymorphisme de l'hydrure de magnesium sous haute pression, Materials Research Bulletin, 15, pp. 1779-1787 (1980).

[19] M. Bortz, B. Bertheville, G. Böettger, K. Yvon, Structure of the high pressure phase γ-MgH_2 by neutron powder diffraction, J. Alloys Comp., 287, pp. L4-6 (1999).

[20] P. Selvam, B. Viswanathan, C.S. Swamy, and V. Srinivasan, Magnesium and magnesium alloy hydrides, International Journal of Hydrogen Energy, 11, pp. 169-192 (1986).

[21] B. Bogdanovic, K. Bohmhammel, B. Christ, A. Reiser, K. Schlichte, R. Vehlen, and U. Wolf, Thermodynamic investigation of the magnesium-hydrogen system, J. Alloys Comp., 282, pp. 84-92 (1999).

[22] J.F. Stampfer, C.E. Holley, and J.F. Suttle, The magnesium-hydrogen system 1-3, Journal of the American Chemical Society, 82, pp. 3504-3508 (1960).

[23] A. Zaluska, L. Zaluski, and J.O. Ström-Olsen, Synergy of hydrogen sorption in ball-milled hydrides of Mg and Mg_2Ni, J. Alloys Comp., 289, pp. 197-206 (1999).

[24] A. Zaluska, L. Zaluski, and J.O. Ström-Olsen, Nanocrystalline magnesium for hydrogen storage, Journal of Alloys and Compounds, 288, pp. 217-225 (1999).

[25] X. Yao, Z.H. Zhu, H.M. Cheng, and G.Q. Lu, Hydrogen diffusion and effect of grain size on hydrogenation kinetics in magnesium hydrides, J. Mater. Res. 23, pp. 336-340 (2008).

[26] Y. Zhang, B.W. Li, H.P. Ren, X. Li, Y. Qi, and D. Zhao, Enhanced hydrogen storage kinetics of nanocrystalline and amorphous Mg_2Ni-type alloy by melt spinning, Materials, 4, pp. 274-287 (2011).

[27] C.D. Yim, B.S. You, Y.S. Na, and J.S. Bae, Hydriding properties of Mg-xNi alloys with different microstructures, Catalysis Today, 120, pp. 276-280 (2007).

[28] T. Spassov, L. Lyubenova, U. Köster, M.D. Baró, Mg-Ni-RE nanocrystalline alloys for hydrogen storage, Mater. Sci. Eng. A, 375-377, pp. 794-799 (2004).

[29] C. Pohlmann, L. Röntzsch, S. Kalinichenka, T. Hutsch, T. Weißgärber, B. Kieback, Hydrogen storage properties of compacts of melt-spun $Mg_{90}Ni_{10}$ flakes and expanded natural graphite, J. Alloys Comp. 509, pp. S625-S628 (2011).

[30] K. Tanaka, Y. Kanada, M. Furuhashi, K. Saito, K. Kuroda, and H. Saka, Improvement of hydrogen storage properties of melt-spun Mg-Ni-RE alloys by nanocrystallization, J. Alloys Comp., 295, pp. 521-525 (1999).

[31] S. Kalinichenka, L. Roentzsch, and B. Kieback, Structural and hydrogen storage properties of melt-spun Mg-Ni-Y alloys, International Journal of Hydrogen Energy, 34, pp. 7749-7755 (2009).

[32] S. Kalinichenka, L. Röntzsch, C. Baehtz, T. Weiβgärber, and B. Kieback, Hydrogen desorption properties of melt-spun and hydrogenated Mg-based

alloys using in situ synchrotron X-ray diffraction and TGA, J. Alloys Comp., 509, pp. S629-S632 (2011).

[33] G. Barkhordarian, T. Klassen, and R. Bormann, Effect of Nb_2O_5 content on hydrogen reaction kinetics of Mg, J. Alloys Comp., 364, pp. 242-246 (2004).

[34] N. Hanada, T. Ichikawa, S. Hino, and H. Fujii, Remarkable improvement of hydrogen sorption kinetics in magnesium catalyzed with Nb_2O_5, J. Alloys Comp., 420, pp. 46-49 (2006).

[35] N. Hanada, T. Ichikawa, and H. Fujii, Catalytic effect of Ni nano-particle and Nb oxide on H-desorption properties in MgH_2 prepared by ball milling, J. Alloys Comp., 404-406, pp. 716-719 (2005).

[36] C.B. Alcock, V.P. Itkin, and M.K. Horrigan, Vapour pressure equations for the metallic elements: 298-2500K, Canadian Metallurgical Quarterly, 23, pp. 309-313 (1984).

[37] X.D. Yi, Rapidly solidified magnesium – nickel alloys as hydrogen storage materials, PhD thesis, University of Birmingham, (2014).

[38] P. Selvam, B. Viswanathan, C.S. Swamay, V. Srinivasan, Thermal studies on Mg_2NiH_4: existence of additional hydride phase in the Mg_2Ni-Hydrogen system. Thermochimica Acta, 125, pp. 1-8 (1988).